inorganics

MDPI

Article

Effect of Doping Inorganic Acid Radical Ions on Electrochemical Properties of Polyaniline/Graphite Carbon Paper Electrodes

Chong Ma [1], Chen Yao [1], Jing Xu [2] and Yibing Xie [1,3,*]

[1] School of Chemistry and Chemical Engineering, Southeast University, Nanjing 211189, China
[2] College of Ecology and Resource Engineering, Wuyi University, Wuyishan 354300, China
[3] Suzhou Research Institute, Southeast University, Suzhou 215123, China
* Correspondence: ybxie@seu.edu.cn

Abstract

The inorganic proton acid-doped polyaniline (H-PANI-X) is synthesized directly on a graphite carbon paper electrode. The polyaniline doped with hydrochloric acid (yielding H-PANI-Cl), sulfuric acid (yielding H-PANI-HSO_4), and nitric acid (yielding H-PANI-NO_3) is employed to construct both finite molecule and periodic molecule computational models. Theoretical calculation and experimental measurement of a polyaniline/graphite carbon paper electrode are adopted to reveal the doping effect of inorganic acid radical ions (Cl^-, HSO_4^-, NO_3^-) on electrical and electrochemical properties of H-PANI-X. H-PANI-X shows a lower electronic band gap structure, indicating more feasible electron transfer than PANI. H-PANI-X shows a lower HOMO-LUMO orbital energy gap, indicating lower excitation energy than PANI. H-PANI-X also shows a higher electronic density of states level, indicating higher electrical conductivity than PANI. The charge density difference of H-PANI-X reveals a more delocalized electrostatic potential distribution, indicating an enhanced electrostatic interaction between protonated PANI and charge-balancing anions. Furthermore, H-PANI-HSO_4 and H-PANI-NO_3 exhibit hydrogen bonding between the protonated PANI and charge-balancing anions, resulting in reduced electronic band gaps and enhanced electronic density of states compared with H-PANI-Cl. H-PANI-NO_3 with higher electronic states at the Fermi level and higher anionic electronegativity exhibits higher electrical conductivity than H-PANI-Cl and H-PANI-HSO_4. The experimental measurement is conducted to investigate the electrochemical properties of H-PANI-X. The electrochemical impedance spectroscopy measurement indicates H-PANI-NO_3 maintains lower charge transfer resistance (0.357 Ω) than H-PANI-HSO_4 (3.003 Ω) and H-PANI-Cl (10.571 Ω). The cyclic voltammetry measurement indicates that H-PANI-NO_3 has much higher redox current and mean current density responses, accordingly exhibiting superior capacitance (208.0 mF cm^{-2}) performance in comparison with H-PANI-Cl (129.5 mF cm^{-2}) and H-PANI-HSO_4 (157.9 mF cm^{-2}). Theoretical calculation and experimental investigation confirm H-PANI-NO_3 presents superior electroactivity to H-PANI-Cl and H-PANI-HSO_4 for promoting its electrochemical capacitance performance.

Keywords: proton acid doping effect; polyaniline; electrochemical; electrical; theoretical calculation

Check for updates

Academic Editor: Duncan H. Gregory

Received: 28 January 2026
Revised: 20 March 2026
Accepted: 21 March 2026
Published: 24 March 2026

Copyright: © 2026 by the authors. Licensee MDPI, Basel, Switzerland. This article is an open access article distributed under the terms and conditions of the Creative Commons Attribution (CC BY) license.

1. Introduction

π-conjugated conductive polymers achieve electrical conductivity through the doping and dedoping process. The doping conductive polymers can be used as electroactive

electrode materials for various electrochemical applications [1]. The affecting factors of dopants and polymers have been fully investigated to reveal the electrical conductivity and electrochemical properties of the doping conductive polymers [1–3]. Two kinds of proton acids are adopted for doping the conducting polymer to achieve electrical conductivity, which include inorganic proton acids (such as HCl, H_2SO_4, and HNO_3) and organic proton acids (such as dodecylbenzene sulfonic acid and p-toluenesulfonate acid) [4–6]. In general, anions derived from inorganic and organic acids can serve as highly effective dopants, exerting a significant influence on the properties of conductive polymers. The doping and dedoping characteristics of poly(3,4-ethylenedioxythiophene)/poly(styrene sulfonate)/poly(vinyl sulfonate) have been thoroughly investigated to reveal the electrochemical properties [7,8]. The electrical performance of poly(3-hexylthiophene) doped with 2,3,5,6-tetrafluoro-7,7,8,8-tetracyanoquinodimethane was reported to demonstrate doping-induced charge transfer in conductive polymers [9]. The electrochemical properties of polypyrrole doped with 1,5-naphthalene disulfonate and 2-naphthalene sulfonate were reported to achieve supercapacitor application [10]. The amino trimethylene phosphonic acid doping effect on polyaniline/carbon nanotube composite was also reported to achieve supercapacitor application [11]. Polypyrrole coupled with chloride and methyl orange anionic dopants was studied for application in high-power lithium-ion batteries [12]. Electrochemical capacitance measurements were conducted to investigate the effects of doping with various organic acids on polypyrrole/carbon nanotube/polyimide composite. Density functional theory calculations have also been employed to explore the electronic properties during the doping and dedoping of conductive polymers [13–16].

Polyaniline (PANI) is a prominent conductive polymer widely utilized as supercapacitor electrode material due to its facile synthesis, excellent electrical activity, and environmental friendliness. Normally, PANI typically exists in three oxidation states which are shown as pernigraniline (comprising one quinoid and one benzenoid unit), emeraldine (consisting of three benzenoid and one quinoid unit), and leucoemeraldine (containing only benzenoid units). As one kind of typical conductive polymer, PANI undergoes the doping and dedoping processes in various electrolyte solutions, facilitating charge and discharge cycles essential for electrochemical energy storage. The choice of electrolytes, which act as dopants, significantly influences the properties of protonated PANI [14,17–19]. A comparative study of the doping effect of organic acid dopants (tartaric acid and oxalic acid) and inorganic acid dopants (hydrochloric acid and perchloric acid) on the electrical properties of polyaniline was performed and reported [20,21]. It was revealed that the inorganic acid dopant of perchloric acid leads to higher conductivity of PANI. The organic acid dopant of tartaric acid causes lower conductivity of PANI [22]. Importantly, inorganic proton acids usually cause superior capacitance due to the feasible protonation and electrostatic interaction process of PANI. The anions originated from proton acid electrolytes would maintain a strong interaction with the protonated PANI through the electrostatic adsorption process, thereby improving overall electrochemical performance [23]. The type of doping ions is closely linked to the electrical and electrochemical properties of the conductive polymers. Among the strong inorganic proton acids, HCl, H_2SO_4, and HNO_3 are considered as optimal doping electrolytes because they provide ample protons for the protonation of PANI. The charge-balancing anions are investigated to reveal the relationship and effect on the electrical properties of the protonated PANI. Theoretical calculation and experimental measurement are adopted to investigate the proton acid (HX) doping effect on the electrochemical performance of PANI. Our previous study fully investigated and reported the electrochemical performance of graphite electrode based on sulfuric acid-doped polyaniline on graphite carbon electrode [24].

In this study, PANI was synthesized on a carbon paper substrate to fabricate PANI/carbon paper composite electrodes. Both theoretical calculation and experimental measurement are employed to investigate the effects of inorganic proton acid doping on the electrical and electrochemical properties of PANI [25–27]. The dispersion-corrected density functional theory (DFT) is utilized to investigate the electrical properties of proton acid doping PANI (H-PANI-X). The density of states (DOS) is calculated to investigate the electrical conductivity of proton acid-doped PANI. The charge density difference analysis is performed to reveal the electrostatic interactions between protonated PANI and charge-balancing anions. The electronic band structure and HOMO-LUMO orbital energy gaps are applied to investigate the electron transfer capability and excitation energy of H-PANI-X. Molecular electrostatic potential is also employed to investigate charge distribution and electron delocalization. The experimental measurement is conducted to investigate the electrochemical properties of H-PANI-X when PANI undergoes the doping and de-doping process in inorganic proton acid electrolyte medium. The theoretical calculation results are verified by the experimental measurement results to confirm the electrical and electrochemical properties of proton acid doping PANI.

2. Theoretical Calculation and Experimental Measurement

2.1. Theoretical Calculation

Definite and periodic molecular models of proton acid HX doping PANI are established and optimized by means of density functional theory-based electronic structure calculation. The generalized gradient approximation (GGA) level of Predew, Burke and Ernzernhof (PBE) are applied to explore density of states (DOS) with the CASTEP package. The highest occupied molecular orbital (HOMO) and lowest unoccupied molecular orbital (LUMO) molecule orbital energy gap and electrostatic potential (ESP) are optimized by the DMol3 package. The cut-off energy is 380 eV. The SCF tolerance is Fine. The OTFG ultrasoft is set at thresholds of the convergence tolerance in pseudopotentials and the Koelling–Harmon is set in relativistic treatment. The electronic band structure and HOMO-LUMO orbital energy gap of H-PANI-X are used to analyze the electron transfer and excitation energy of H-PANI-X. Density of states (DOS) calculations are performed to investigate the electrical conductivity of H-PANI-X. Charge density difference analysis is conducted to characterize the electrostatic interactions between protonated polyaniline and charge-compensating anions.

2.2. Experimental Measurement

Electrochemical measurements are performed in a three-electrode system. Inorganic proton acid HX doping PANI/carbon paper (H-PANI-Cl, H-PANI-HSO_4 and H-PANI-NO_3) serves as the working electrode, a Pt sheet is used as the counter electrode, and an SCE electrode is used as the reference electrode. Aqueous solution of 1.0 M HCl, 1.0 M H_2SO_4, or 1.0 M HNO_3 is used as the electrolyte. Electrochemical measurements, including cyclic voltammetry (CV) and electrochemical impedance spectroscopy (EIS), were performed using a CHI 760C electrochemical workstation (Shanghai, China). The chemicals of HCl, H_2SO_4, HNO_3 are analytical grade and are purchased from China National Pharmaceutical Group Co., Ltd. (Shanghai, China). Concerning the preparation and electrodeposition procedure, the potential range of −0.2~1.0 V, scan rate of 25 mV s^{-1} and sweep segments of 10 cycles were applied during the CV electrodeposition. The current density values were normalized to the geometric surface area of the electrode.

3. Results and Discussion

3.1. Simulation Calculation

Figure 1a–h show finite molecular models of PANI, H-PANI-Cl, H-PANI-HSO_4 and H-PANI-NO_3 without and with geometric structure optimization. Concerning finite molecular models of PANI, H-PANI-Cl, H-PANI-HSO_4 and H-PANI-NO_3, aniline monomer unit structure has occurred the angle torsion from the coplanar structure to the twisting structure, which is due to the geometric structure optimization. The characteristic unit of the model molecular structure of proton acid-doped polyaniline involves the protonated imino group (=NH^+−), which maintains an electrostatic interaction with the doping anions, such as Cl^-, HSO_4^- and NO_3^-.

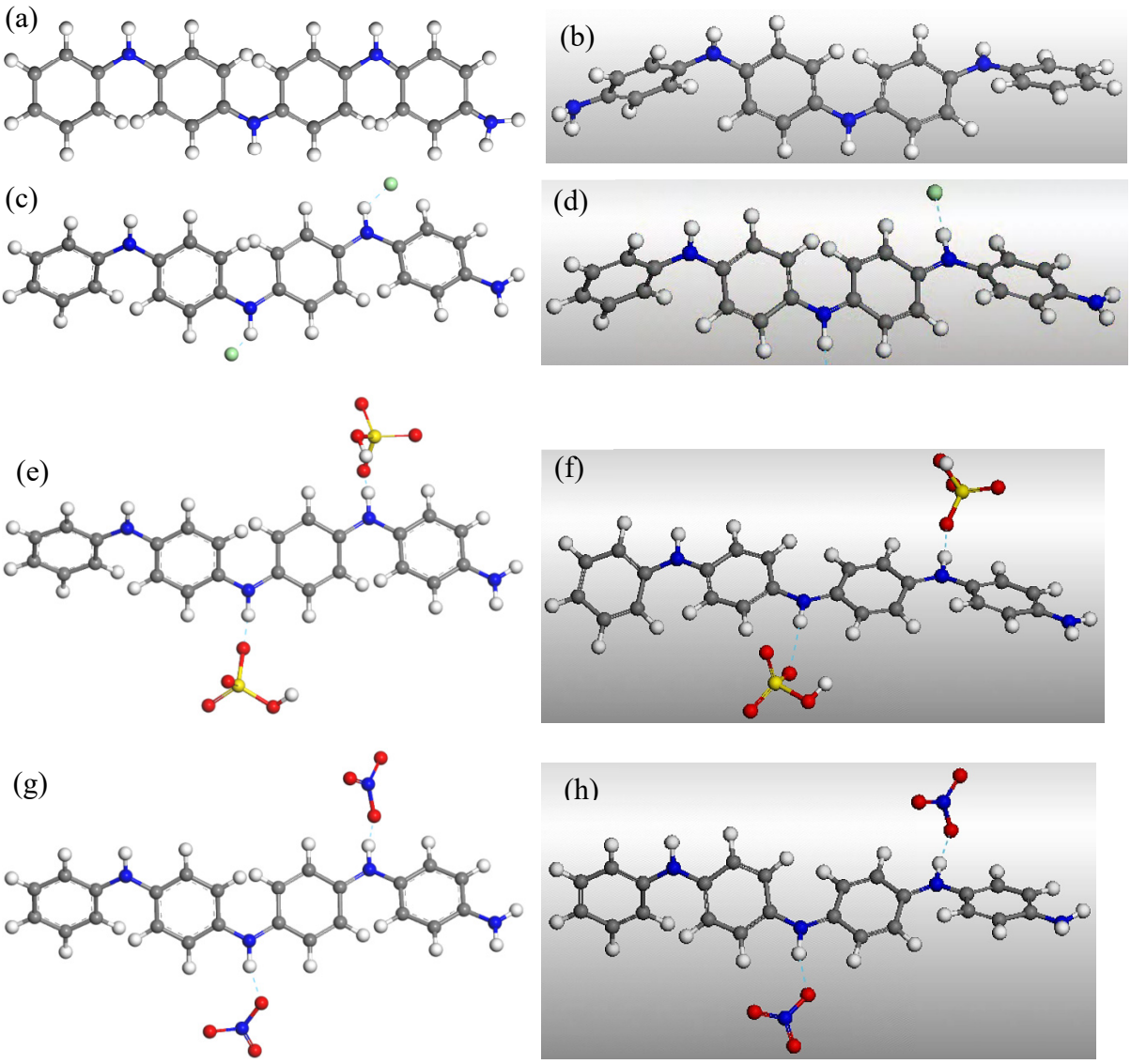


Figure 1. Finite molecular models of (**a**,**b**) H-PANI, (**c**,**d**) H-PANI-Cl, (**e**,**f**) H-PANI-HSO_4 and (**g**,**h**) H-PANI-NO_3 without and with geometric structure optimization.

Figure 2a–d show the electrostatic potential distribution (ESP) on the electron density isosurface of PANI, H-PANI-Cl, H-PANI-HSO_4 and H-PANI-NO_3. The ESP analysis of the molecular charge distribution is a feasible method to investigate the electrostatic potential of molecules. The ESP energy is calculated at each point on the molecular surface, which is equal to the interaction energy between the molecular charge distribution and a positive

charge unit located at this point. Generally, it is more likely to undergo an electrophilic reaction when the atom is closer to the point of the lowest electrostatic potential on the van der Waals surface. Similarly, it is more likely to undergo a nucleophilic reaction when the atom is closer to the point of the highest electrostatic potential on the van der Waals surface. The electrostatic potential calculation results show that PANI, H-PANI-Cl, H-PANI-HSO_4 and H-PANI-NO_3 involve the positive potential distribution on the hydrogen atoms of the benzene ring, benzoquinone ring, and imino group. PANI involves negative potential distribution on the carbon atoms of the conjugated benzene rings and quinone nitrogen atoms of π-conjugated polymer chain. In comparison, H-PANI-Cl, H-PANI-HSO_4, and H-PANI-NO_3 exhibit negative potential main distribution on the charge-balancing anions, along with partial distribution on the nitrogen atoms. The increased positive potential remains localized on the hydrogen atoms. Compared with pristine PANI, the electrophilic regions of H-PANI-Cl, H-PANI-HSO_4, and H-PANI-NO_3 are still concentrated on the hydrogen atoms, while their nucleophilic regions are distributed on the corresponding anions. Thus, protonation doping and anion interaction induce charge transfer from the conjugated benzene rings of PANI to the electrostatic charge-balancing anions of H-PANI-Cl, H-PANI-HSO_4 and H-PANI-NO_3. This indicates a strong electrostatic interaction between the protonated PANI and charge-balancing anions of Cl^-, HSO_4^-, and NO_3^-.

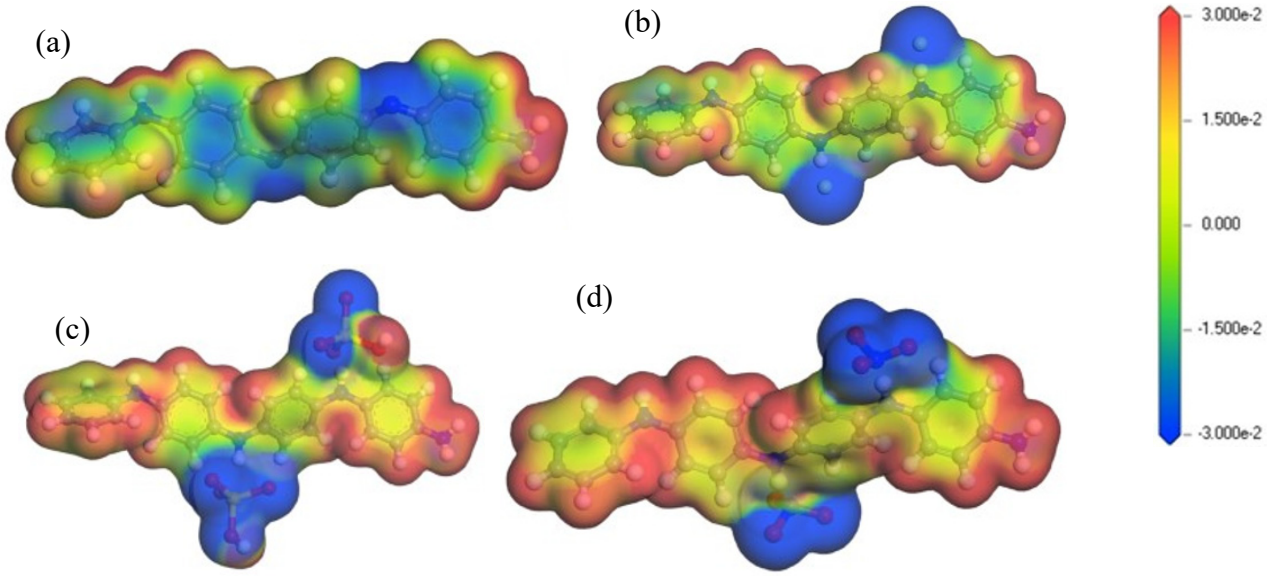


Figure 2. Electrostatic potential on electron density isosurface of (**a**) PANI, (**b**) H-PANI-Cl, (**c**) H-PANI-HSO_4 and (**d**) H-PANI-NO_3.

Frontier molecular orbital theory is applied to investigate HOMO and LUMO orbital energy, reflecting excitation energy, conductivity and structural stability. Table 1 shows the HOMO and LUMO frontier molecular orbital energy of PANI, H-PANI-Cl, H-PANI-HSO_4 and H-PAN-NO_3. The theoretical calculation results show that H-PANI-X has lower HOMO and LUMO orbital energy than PANI, indicating better structural stability. H-PANI-X also has a lower HOMO-LUMO orbital energy gap than PANI, indicating its lower excitation energy, stronger electron transfer capacity, and higher conductivity. Furthermore, H-PAN-NO_3 shows a lower HOMO-LUMO orbital energy gap than H-PANI-Cl and H-PANI-HSO_4. H-PANI-NO3 has the strongest electron transfer capability from HOMO to LUMO. It is believed that charge-balancing anions modulate the HOMO and LUMO orbital energy levels, thereby lowering HOMO-LUMO orbital energy gap.

Table 1. Frontier molecular orbital HOMO and LUMO orbital energy, and HOMO-LUMO energy gap of PANI, H-PANI-Cl, H-PANI-HSO_4 and H-PAN-NO_3.

Molecule	HOMO Orbital Energy (eV)	LUMO Orbital Energy (eV)	HOMO-LUMO Orbital Energy Gap (eV)
PANI	−2.78	−3.96	1.18
H-PANI-Cl	−4.63	−4.02	0.62
H-PANI-HSO_4	−5.25	−4.00	0.45
H-PANI-NO_3	−5.03	−4.80	0.23

The Fukui index is used to study the chemical reactive sites and strength of molecules. The electrophilic attack index indicates the strength of the electron giving ability of the atom in a molecule. The nucleophilic attack index indicates the strength of the electron gaining ability of the atom in a molecule. Figure 3 shows the electrophilic aggression index and nucleophilic aggression index of H-PANI, H-PANI-Cl, H-PANI-HSO_4 and H-PANI-NO_3. The N atoms in PANI are the main reactive sites, which are the attack sites of electrophilic reactions and nucleophilic reactions. Comparatively, H-PANI-Cl, H-PANI-HSO_4 and H-PANI-NO_3 show significantly lower electrophilic and nucleophilic aggression indices at N1 and N2 atoms. So, PANI is prone to electrophilic substitution reaction and nucleophilic substitution reaction in comparison with H-PANI-Cl, H-PANI-HSO_4 and H-PANI-NO_3.

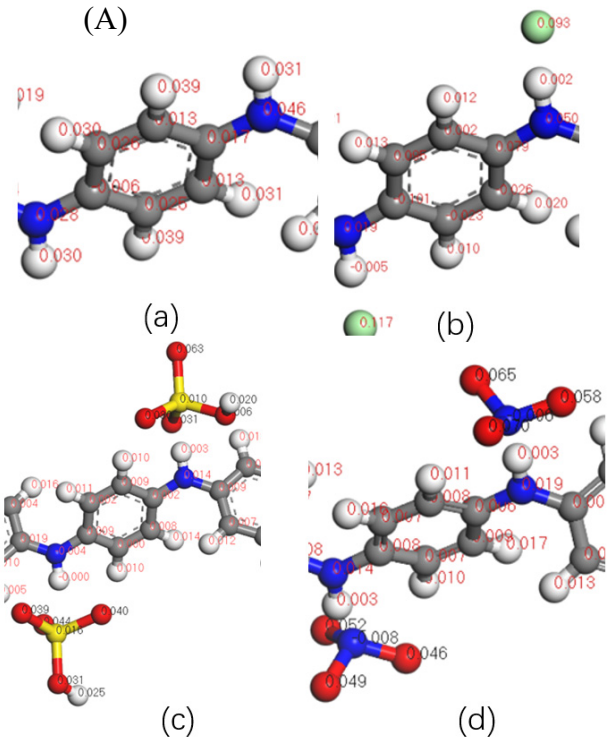


Figure 3. *Cont.*

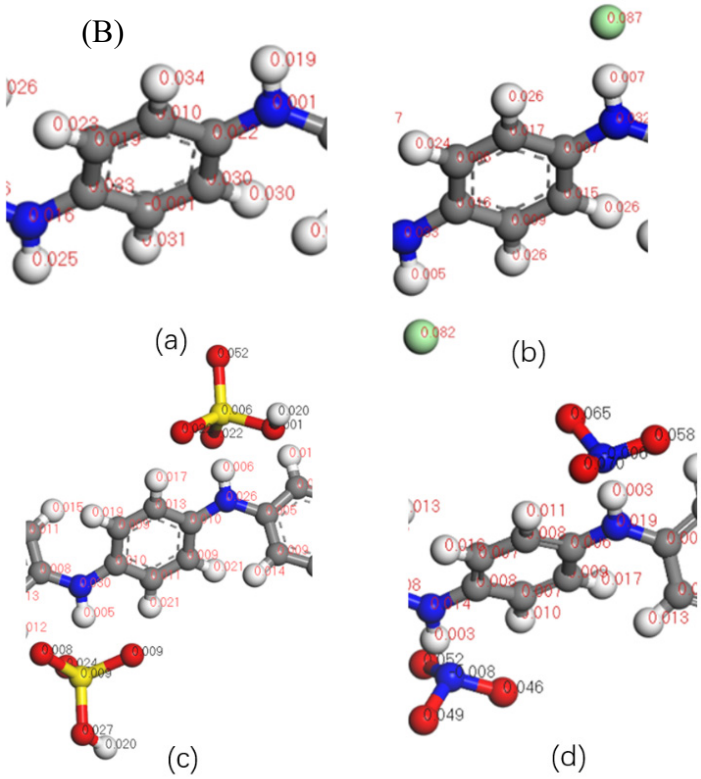


Figure 3. (**A**) Electrophilic and (**B**) nucleophilic aggression index of (**a**) PANI, (**b**) H-PANI-Cl, (**c**) H-PANI-HSO_4, and (**d**) H-PANI-NO_3.

Figure 4a–d show the Mulliken charge distribution of H-PANI, H-PANI-Cl, H-PANI-HSO_4 and H-PANI-NO_3. It involves the following characteristics. Concerning the charge distribution of PANI, the negative potential is evenly distributed on the backbone of nitrogen atoms of the imino group on the π-conjugated polymer chain, while the positive potential is mainly distributed on the hydrogen atoms and some carbon atoms on the benzene ring. Concerning the protonation effect, the negative potential of nitrogen atom is stronger, while the positive potential change on hydrogen and carbon atom is not so significant. Concerning the charge distribution of H-PANI-Cl, the negative potential is mainly located on chloride ions, and the negative potential of nitrogen atoms on H-PANI-Cl is similar to PANI. The positive potential is still concentrated on the hydrogen atoms and several carbon atoms. Concerning the charge distribution of H-PANI-HSO_4, the negative potential of nitrogen atoms on H-PANI-HSO_4 is similar to that of PANI. Compared with H-PANI-Cl, H-PANI-HSO_4 shows lower negative potential on the benzene rings and nitrogen atoms. Positive potential is still distributed on the hydrogen atom and part of the carbon atom. For H-PANI-NO_3, the negative potential remains predominantly localized on the anion, whereas the positive potential is concentrated on the hydrogen atoms and several carbon atoms. Compared with H-PANI-Cl and H-PANI-HSO_4, H-PANI-NO_3 showed weaker negative potential on the benzene rings as well as on the nitrogen atoms. Meanwhile, H-PANI-NO_3 shows a greater delocalization of charge density distribution and a higher electrical conductivity.

The electrical properties of H-PANI-X are highly dependent on molecular configuration, in which charge-balancing anions interact with adjacent protonated imino groups. Figure 5a–d show periodic molecular models of PANI, H-PANI-Cl, H-PANI-HSO_4, and H-PANI-NO_3. The circles around sections of the periodic molecular models denote the electrostatic interaction between the protonated PANI and charge-balancing anions. Specifically,

the doping anions could interact with the protonated imino groups on the benzoquinone ring of PANI, which causes the formation of the protonation acid-doped PANI.

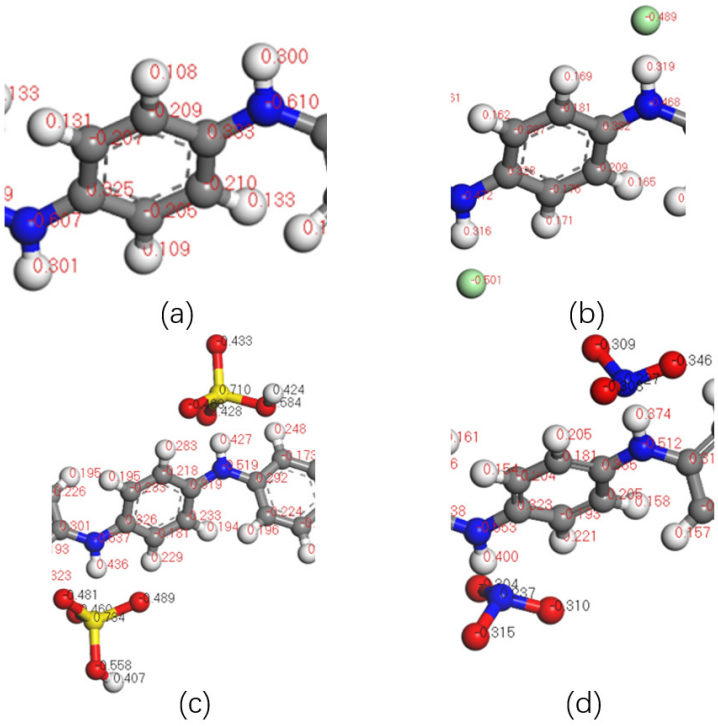


Figure 4. Mulliken charge distribution of (**a**) PANI, (**b**) H-PANI-Cl, (**c**) H-PANI-HSO_4, and (**d**) H-PANI-NO_3.

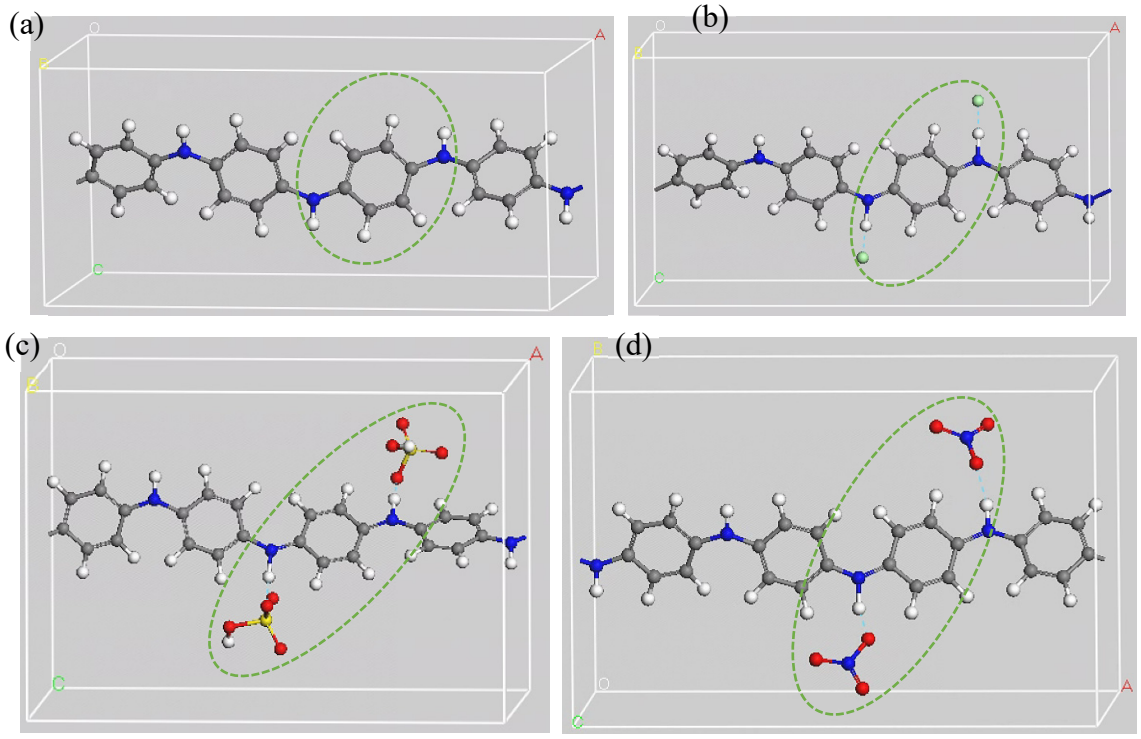


Figure 5. (**a**–**d**) Periodic molecular models of PANI, H-PANI-Cl, H-PANI-HSO_4, and H-PANI-NO_3.

Geometric optimization of molecular configuration aims to achieve a lowered energy state and enhanced structural stability. The main changes in geometric configuration occur on the ring plane angle and carbon/nitrogen bond length of the neighboring benzene rings

of the PANI periodic molecule. Figure 6a,b show the geometric configuration of the PANI periodic molecular model without and with structure optimization. Figure 6c shows atomic labeling in the PANI periodic molecule. Table 2 provides a parameter comparison of the ring plane angle and bond length in the geometric configuration of the PANI periodic molecule. Notably, the plane angle of the benzene torus shows almost no change. However, the plane angle of adjacent benzene rings linked by nitrogen atoms increases from 23.014° to 24.079° in the optimized periodic molecule structure. The interatomic distance between carbon and nitrogen atoms decreases from approximately 1.513 Å to 1.412 Å. Due to the planar opening of the benzene ring, the interatomic distance between neighboring hydrogen atoms also increases from 1.383 Å to 2.169 Å. So, the decreased C-N bonding distance and the increased plane angle of benzene rings result in the enhanced structural stability of the optimized periodic molecule.

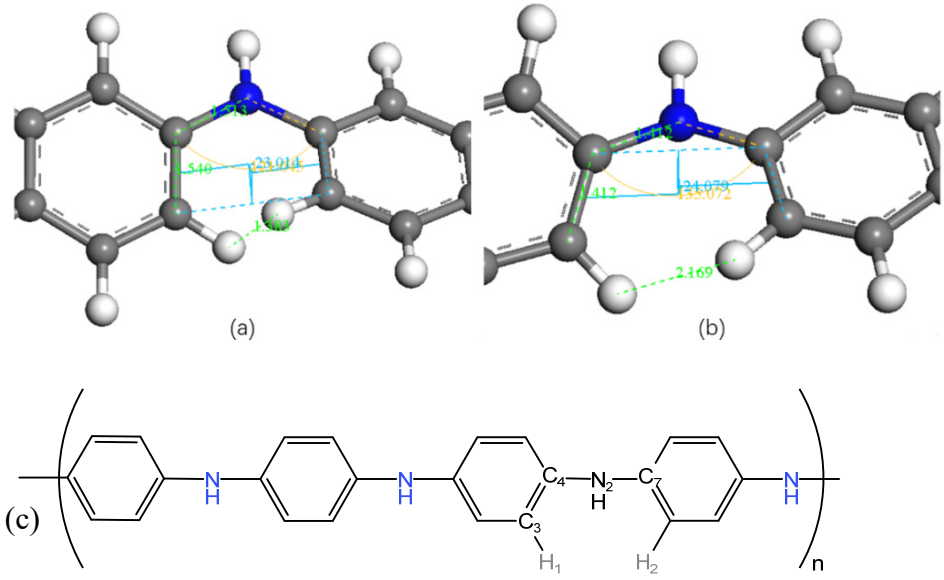


Figure 6. (**a**,**b**) Geometric configuration of PANI periodic molecular model without and with structure optimiza-tion; (**c**) atomic labeling in PANI periodic molecule.

Table 2. Parameter comparison of ring plane and interatomic distance in geometric configuration of PANI periodic molecule.

Parameters (r, Interatomic Distance, Å; α, Ring Plane Angle, °)	PANI Without Optimization	PANI With Optimization
r (C3-C4)	1.540	1.412
r (C4-N2)	1.513	1.412
r (H1-H2)	1.383	2.169
α (benzene ring plane)	23.014	24.079

Figure 7a–d show the electronic band structure curves of PANI, H-PANI-Cl, H-PANI-HSO_4 and H-PANI-NO_3. The electronic band gaps of PANI, H-PANI-Cl, H-PANI-HSO_4 and H-PANI-NO_3 are determined to be 2.227, 0.773, 0.592 and 0.491 eV, respectively. H-PANI-Cl, H-PANI-HSO_4 and H-PANI-NO_3 show a much lowered band gap structure when compared with PANI. Thus, proton acid doping can significantly enhance the electrical conductivity of H-PANI-X. Furthermore, H-PANI-HSO_4 and H-PANI-NO_3 show lower band gaps than H-PANI-Cl. Moreover, the formation of hydrogen-bonding structures in H-PANI-HSO_4 and H-PANI-NO_3 significantly strengthens the electrostatic interactions between protonated PANI and charge-balancing anions of HSO_4^- and NO_3^-. Accordingly,

the electron transfer process in H-PANI-HSO_4 and H-PANI-NO_3 becomes more favorable, resulting in higher electrical conductivity.

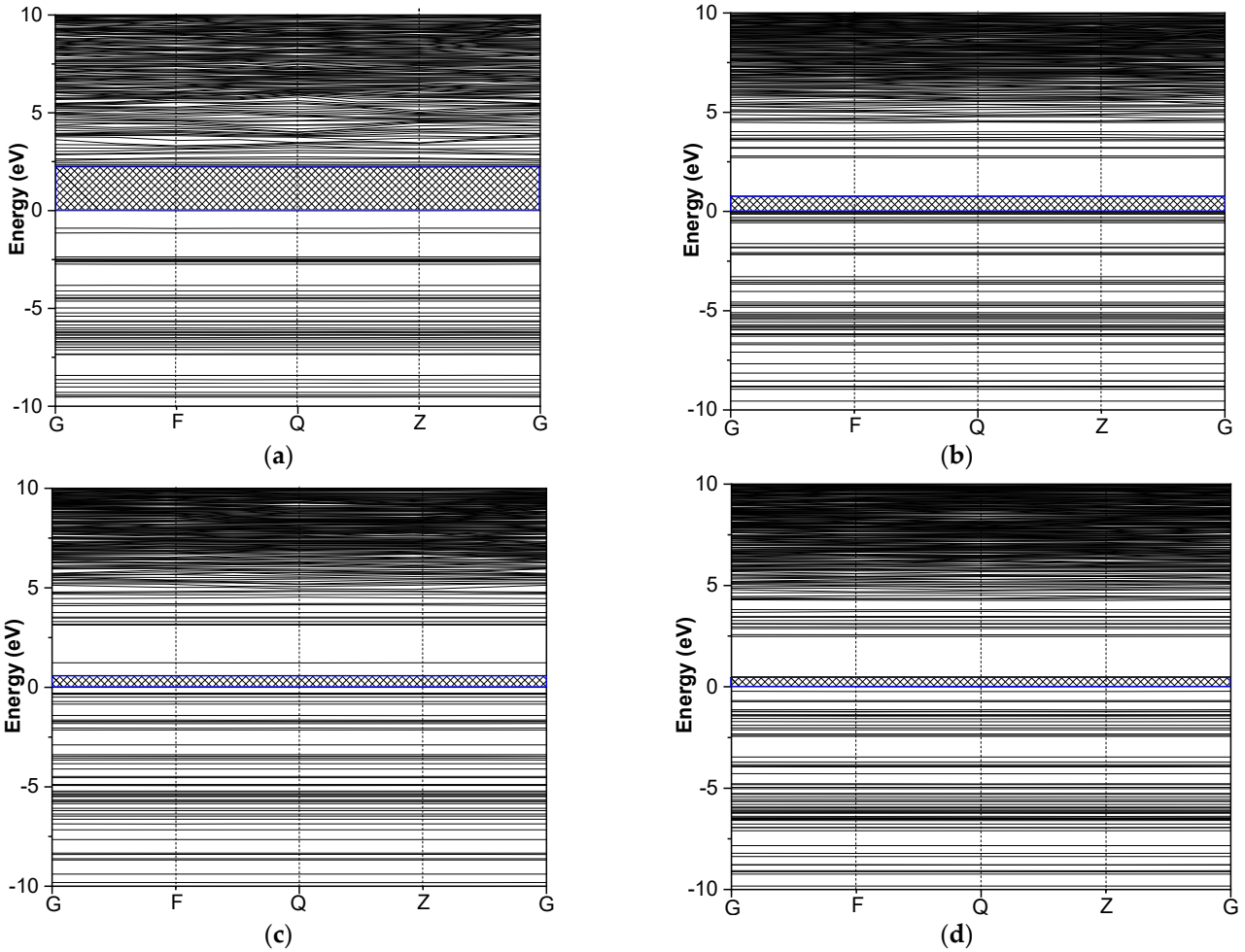


Figure 7. Electronic band structure curves of (**a**) PANI, (**b**) H-PANI-Cl, (**c**) H-PANI-HSO_4, and (**d**) H-PANI-NO_3.

Figure 8a,b show the density of states curves and number of electronic states at the Fermi level for PANI, H-PANI-Cl, H-PANI-HSO_4, and H-PANI-NO_3. Herein, the density of states (DOS) at the Fermi level, expressed as N(E), can be used to assess the electrical conductivity of H-PANI-X. N(E) represents the quantity of distinct quantum states available to electrons at a specific energy level, which precisely indicates the number of electronic states per unit volume and per unit energy. The DOS characterizes the distribution of electronic states with respect to energy and is mathematically defined as D(E) = N(E)/V, where N(E) denotes the number of states within an infinitesimal energy range E to E + δE in a system of volume V. The vertical dashed line represents the density of states at the Fermi level. The valence band lies below the Fermi level, while the conduction band lies above the Fermi level. The electronic band gap represents the minimum energy required for electron excitation and electron transition from valence band to conduction band. The increased density of states at the Fermi level indicates a corresponding enhancement in electron conductivity. The density of states at the Fermi level, expressed as N(E), can be used to assess electrical conductivity of polymers. According to Mott's variable range transition conduction theory, the relationship between N(E) and conductivity (σ) can be expressed as the following equation.

$$\sigma = e^2 v \left[\frac{9N(E)}{8\pi\alpha k_B T}\right]^{1/2} e^{-\left[\frac{\rho\alpha^3}{k_B T N(E)}\right]^{1/4}} \quad (1)$$

where σ is the conductivity as a state density function of Fermi level N(E) and thermodynamic temperature T (298 K), e is the electron charge, v represents the transition frequency, α represents the reciprocal of the rate of decline of the wave function, kB is the Boltzmann constant, and ρ (≈18.1) is the scalar constant. At a constant temperature, the σ value of the polymer is positively correlated with N(E). The calculation shows that the density of states at the Fermi level of PANI, H-PANI-Cl, H-PANi-HSO_4 and H-PANI-NO_3 are 4.17 eV, 7.99 eV, 10.61 eV and 18.32 eV, respectively. The electrical conductivity of the polymer is positively correlated with the electron state level at the Fermi level when the temperature is constant. The narrower band gap signifies more favorable electron transfer and thus higher electrical conductivity. The DOS calculation results show that the number of electronic states of PANI, H-PANI-Cl, H-PANI-HSO_4 and H-PANI-NO_3 increases sequentially at the Fermi level. This indicates that the highest occupied molecular orbitals involve more electron occupation, leading to the increased possibility of electron transition. Higher DOS values are related to higher electrical conductivity.

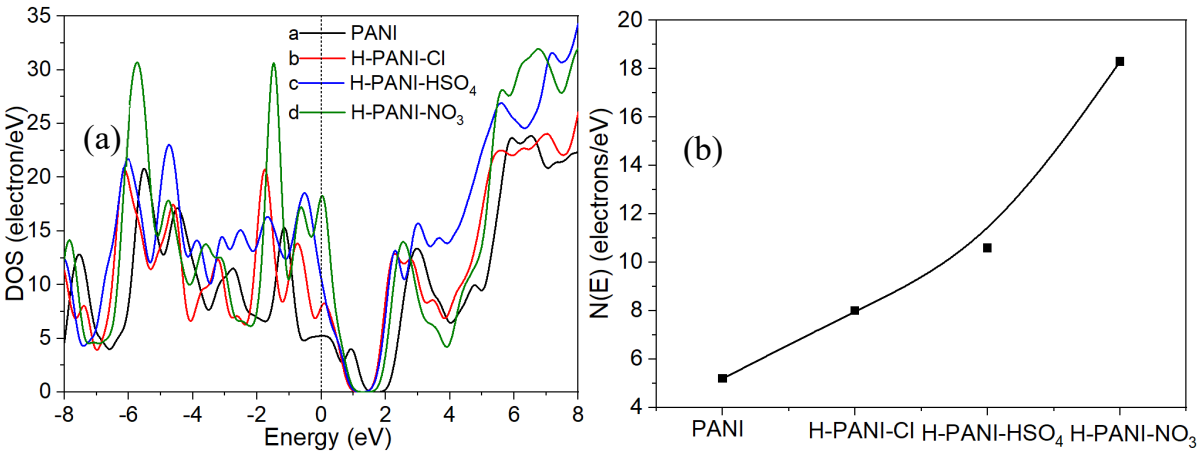


Figure 8. (**a**) Density of states curves and (**b**) number of electronic states at Fermi level for PANI, H-PANI-Cl, H-PANI-HSO_4, and H-PANI-NO_3.

3.2. Experimental Measurement

Figure 9a shows an SEM image of PANI grown on graphite carbon paper. For PANI supported on graphite carbon paper, the PANI layer consists of interconnected nanowires forming a network structure. The overlapping nanowires result in the formation of a porous structure [28,29]. Figure 9b shows a Raman spectrum of PANI grown on graphite carbon paper. Concerning graphite carbon, the Raman peak at 1592 cm^{-1} corresponds to the G band of graphite carbon paper, which is assigned to the E_{2g} vibrational mode of the sp^2 hybrid carbon in graphite. The Raman peak at 1347 cm^{-1} corresponds to the D band of graphite carbon paper, which is assigned to the A_{1g} vibrational mode of the sp^3 hybrid carbon in graphite. Accordingly, graphite carbon paper has the lowered in-plane sp^2-hybrid carbon domains, which were partially converted into sp^3-hybrid carbon. This indicates that graphite carbon paper mostly retains good crystallinity of graphite in the PANI/carbon paper electrode. Concerning polyaniline, the Raman peaks that appeared in the wave number range of 1100–1700 cm^{-1} correspond to the stretching modes of different bonds. The Raman band at 1617 cm^{-1} is assigned to the C–C stretching vibration of the benzene ring. The Raman band at 1497 cm^{-1} is assigned to the N–H deformation vibration. The Raman band at 1326 cm^{-1} is assigned to the stretching vibration of polaronic C–N+.

The Raman band at 1266 cm^{-1} is assigned to the C–N stretching vibration of polaronic PANI. The Raman band observed at 1167 cm^{-1} is assigned to the C–H vibration of aromatic rings. The Raman bands from 800 to 1000 cm^{-1} correspond to the in-plane and out-plane deformation vibrations of the benzene rings in the protonated PANI [24,30,31]. So, this suggests the PANI retains the presence of an emeraldine salt state in the PANI/carbon paper electrode.

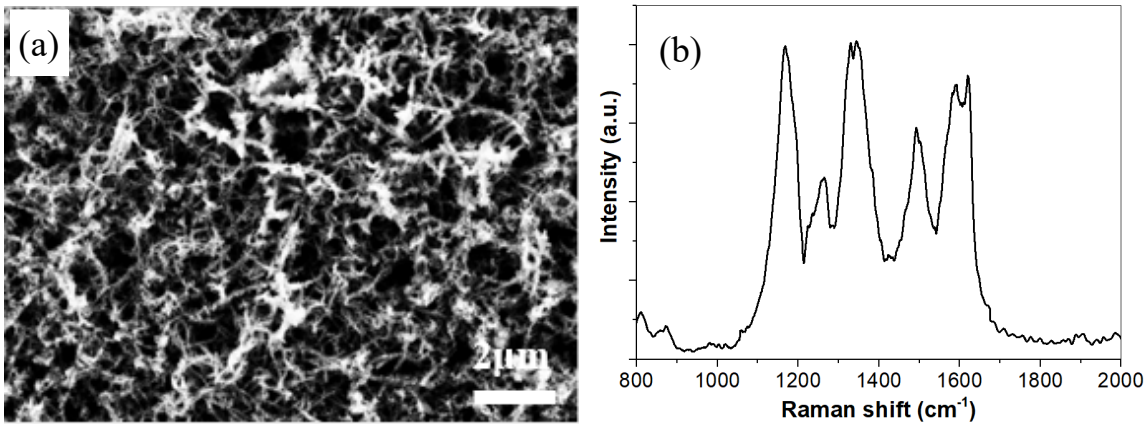


Figure 9. (**a**) SEM image and (**b**) Raman spectrum of PANI grown on graphite carbon paper.

Figure 10 shows the CV curve, capacitance curve and EIS curve and equivalent circuit modeling plot of H-PANI-Cl, H-PANI-HSO_4 and H-PANI-NO_3. Concerning the CV curves, one pair of redox peaks is observed at the oxidation potential of 0.23~0.25 V and the reduction potential of 0.04~0.05 V, which is ascribed to the reversible proton doping and dedoping process of PANI in HCl, H_2SO_4 and HNO_3 electrolyte solutions. The simultaneous electrostatic interaction between protonated PANI and charge-balancing anions of Cl^-, NO_3^- and HSO_4^- gives rise to the formation of H-PANI-Cl, H-PANI-HSO_4, and H-PANI-NO_3. The corresponding oxidation peak current density increases from 3.63 to 4.76 and 5.92 mA cm^{-2}. The symmetric characteristics of the redox are also ascribed to the reversible proton doping and dedoping process of H-PANI-Cl, H-PANI-HSO_4 and H-PANI-NO_3. Accordingly, the specific capacitance of H-PANI-Cl declines from 129.5 to 111.3 mF cm^{-2} when the mean current density increases from 2.59 to 11.14 mA cm^{-2}, revealing a retention rate of 85.9% at a current density ratio of 4.3. The specific capacitance of H-PANI-HSO_4 declines from 157.9 to 143.5 mF cm^{-2} when the mean current density increases from 3.16 to 14.35 mA cm^{-2}, revealing a retention rate of 90.8% at a current density ratio of 4.5. The specific capacitance of H-PANI-NO_3 declines from 208.0 to 173.5 mF cm^{-2} when the mean current density increases from 4.16 to 17.35 mA cm^{-2}, revealing a retention rate of 83.4% at current density ratio of 4.2. The electrochemical impedance spectroscopy (EIS) curves are composed of the semi-circle curves at high-frequency range and linear segments at low-frequency range. The elements of the equivalent circuit model include charge transfer resistance, ohmic resistance, electric double-layer capacitance, and Warburg impedance. According to the fitting parameters of the elements of the equivalent circuit model in the EIS curves, H-PANI-Cl, H-PANI-HSO_4 and H-PANI-NO_3 show similar ohmic resistance R_o values at the range of 1.252~1.153 Ω. Comparatively, H-PANI-NO_3 shows a much lower R_{ct} value (0.357 Ω) than H-PANI-HSO_4 (3.003 Ω) and H-PANI-Cl (10.571 Ω), indicating a more feasible charge transfer occurred in H-PANI-NO_3. Accordingly, H-PANI-NO_3 exhibits superior capacitance (208.0 mF cm^{-2}) performance in comparison with H-PANI-Cl (129.5 mF cm^{-2}) and H-PANI-HSO_4 (157.9 mF cm^{-2}).

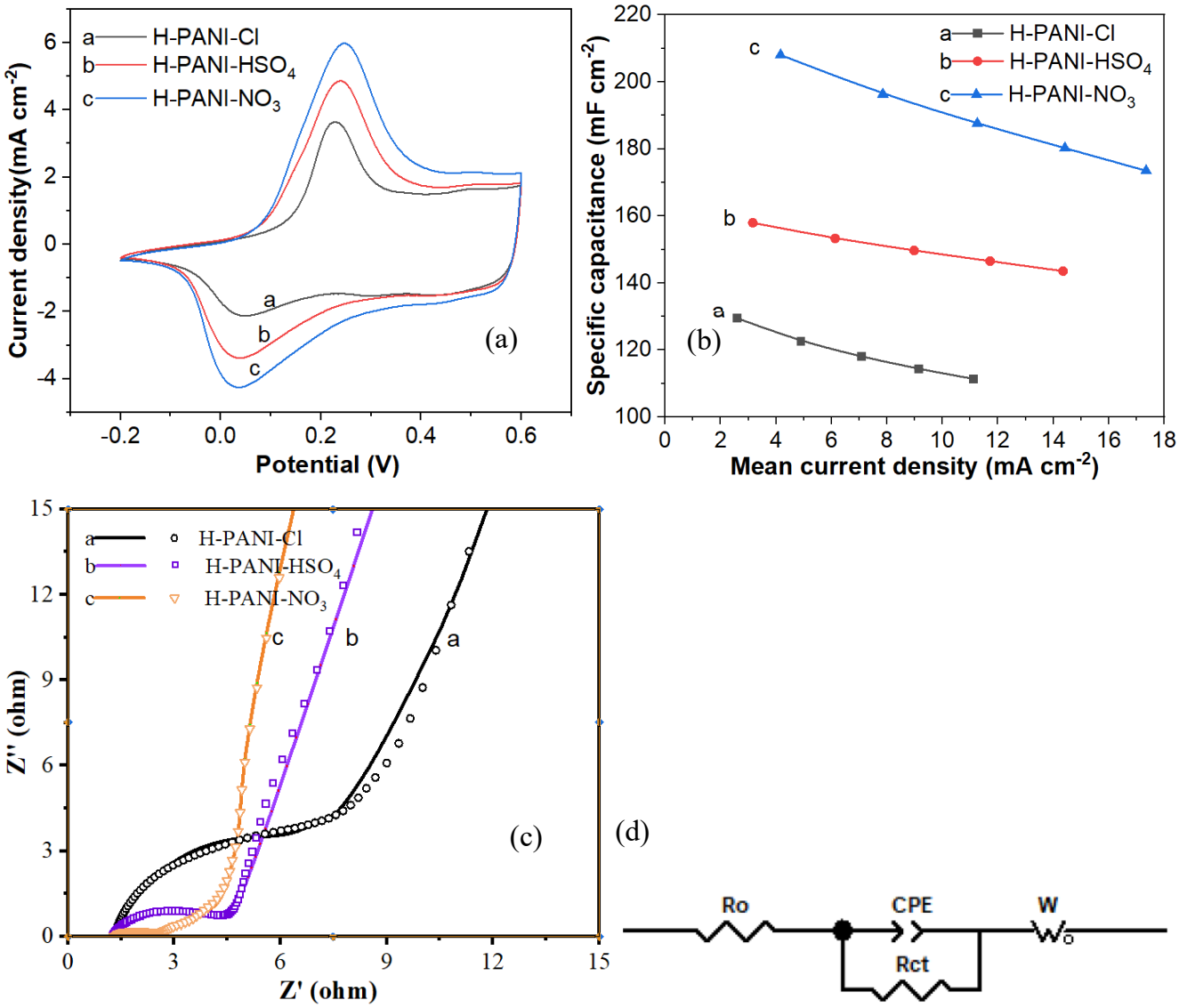


Figure 10. (**a**) CV curve, (**b**) capacitance curve, (**c**) EIS curve, and (**d**) equivalent circuit modeling plot of H-PANI-Cl, H-PANI-HSO_4 and H-PANI-NO_3.

The anionic electronegativity of Cl^- HSO_4^- and NO_3^- was determined to be 3.09, 3.27 and 3.34. Both HSO_4^- and NO_3^- form hydrogen bonding with protonated PANI, yielding stronger electrostatic interactions than Cl^-. NO_3^- exhibits higher electronegativity than HSO_4^-, resulting in stronger electrostatic interaction. Thus, H-PANI-NO_3 shows superior electroactivity compared with H-PANI-Cl and H-PANI-HSO_4.

4. Conclusions

The electrical and electrochemical properties of three inorganic proton acid-doped PANI samples (H-PANI-Cl, H-PANI-HSO_4, and H-PANI-NO_3) supported on graphite carbon paper electrodes were investigated using dispersion-corrected density functional theory calculations and electrochemical measurements, aiming to reveal the doping effects of different proton acids. The state of density, electronic band structure, and HOMO-LUMO orbital energy gap of molecular models are applied to investigate the structural stability and electrical conductivity of H-PANI, H-PANI-Cl, H-PANI-HSO_4 and H-PANI-NO_3. The ESP is applied to study the charge distribution and electron delocalization of modeling molecules. The CV measurement is applied to investigate electrochemical capacitance properties.

The theoretical calculation results show that H-PANI-X, with a lower HOMO and LUMO orbital energy, has better structural stability and lower HOMO-LUMO orbital energy gaps than PANI. The HOMO-LUMO energy gaps of H-PANI-X follow a decreasing order from H-PANI-Cl to H-PANI-HSO_4 to H-PANI-NO_3. H-PANI-NO_3 exhibits stronger electrical conductivity and reactivity than H-PANI-Cl and H-PANI-HSO_4. The Fukui index calculation results show H-PANI-Cl, H-PANI-HSO_4 and H-PANI-NO_3 have significantly lowered electrophilic and nucleophilic aggression indices at nitrogen atoms in comparison with PANI. Mulliken population analysis reveals that H-PANI-NO_3 exhibits weaker negative potentials on both benzene rings and nitrogen atoms compared with H-PANI-Cl and H-PANI-HSO_4, implying more delocalization of charge density distribution and higher electrical conductivity. The density of states at the Fermi level of H-PANI, H-PANI-Cl, H-PANI-HSO_4 and H-PANI-NO_3 is 5.24 eV, 7.99 eV, 10.61 eV and 18.32 eV, respectively. The electrical conductivity of the H-PANI-X follows a successively increasing order for PANI, H-PANI-Cl, H-PANI-HSO_4 and H-PANI-NO_3. The electrochemical measurement results of the polyaniline/graphite carbon paper electrode show H-PANI-NO_3 has a much lower R_{ct} value (0.357 Ω) than H-PANI-HSO_4 (3.003 Ω) and H-PANI-Cl (10.571 Ω), indicating more feasible charge transfer occurred in H-PANI-NO_3. H-PANI-NO_3 exhibits superior capacitance performance when compared with H-PANI-Cl and H-PANI-HSO_4. The theoretical calculation and experimental investigation confirm H-PANI-NO_3 presents superior electroactivity to H-PANI-Cl and H-PANI-HSO_4 for promoting its electrochemical capacitance performance.

Author Contributions: Validation, J.X.; Investigation, C.M.; Writing—review & editing, Y.X.; Supervision, C.Y. and Y.X. All authors have read and agreed to the published version of the manuscript.

Funding: This research work is supported by the Science and Technology Program of Suzhou City, China (SYG202342), and the Big Data Computing Center of the Southeast University, China.

Institutional Review Board Statement: Not applicable.

Informed Consent Statement: Not applicable.

Data Availability Statement: The original contributions presented in this study are included in the article. Further inquiries can be directed to the corresponding author.

Conflicts of Interest: There are no conflicts to declare.

References

1. Pooja, A.; Kumar, A.; Prasher, P.; Mudila, H. Factors affecting the electrical conductivity of conducting polymers. *Carbon Lett.* **2023**, *33*, 307–324. [CrossRef]
2. Lu, Y.; Yu, Z.-D.; Liu, Y.; Ding, Y.-F.; Yang, C.-Y.; Yao, Z.-F.; Wang, Z.-Y.; You, H.-Y.; Cheng, X.-F.; Tang, B.; et al. The Critical Role of Dopant Cations in Electrical Conductivity and Thermoelectric Performance of n-Doped Polymers. *J. Am. Chem. Soc.* **2020**, *142*, 15340–15348. [CrossRef]
3. Bednarczyk, K.; Matysiak, W.; Tański, T.; Janeczek, H.; Schab-Balcerzak, E.; Libera, M. Effect of polyaniline content and protonating dopants on electroconductive composites. *Sci. Rep.* **2021**, *11*, 7487. [CrossRef]
4. Anwar, N.; Shakoor, A.; Ali, G.; Ahmad, H.; Niaz, N.A.; Irfan, M.; Bibi, A. Preparation and characterization of polyaniline–dodecylbenzene sulfonic acid–cadmium oxide (PANI-DBSA-CdO) composites: As an electrode material for energy storage applications. *Polym. Bull.* **2025**, *82*, 3109–3129. [CrossRef]
5. Omar, S.N.I.; Ariffin, Z.Z.; Akhir, R.A.M.; Shri, D.N.A.; Halim, M.I.A.; Safian, M.F.; Azman, H.H.; Ramli, R.; Mahat, M.M. Polyaniline (PANI) fabric doped p-toluene sulfonic acid (pTSA) with anti-infection properties. *Mater. Today Proc.* **2019**, *16*, 1994–2002. [CrossRef]
6. Kulkarni, M.V.; Viswanath, A.K.; Aiyer, R.C.; Khanna, P.K. Synthesis, characterization, and morphology of p-toluene sulfonic acid-doped polyaniline: A material for humidity sensing application. *J. Polym. Sci. Part B Polym. Phys.* **2005**, *43*, 2161–2169. [CrossRef]

7. Eun, J.; Kim, D.; Kim, F.S. Electrochemical Doping and Dedoping Behaviors of PEDOT-Based Ternary Conducting Polymer Composites with Binary Polymer Surfactants. *ACS Appl. Polym. Mater.* **2023**, *5*, 5495–5502. [CrossRef]
8. Magalhaes, C.; Ribeiro, A.I.; Rodrigues, R.; Meireles, A.; Alves, A.C.; Rocha, J.; de Lima, F.P.; Martins, M.; Mitu, B.; Satulu, V.; et al. DBD plasma-treated polyester fabric coated with doped PEDOT:PSS for thermoregulation. *Appl. Surf. Sci.* **2025**, *686*, 162152. [CrossRef]
9. Luo, S.; Xu, Z.; Zhong, F.; Li, H.; Chen, L. Doping-induced charge transfer in conductive polymers. *Chin. Chem. Lett.* **2024**, *35*, 109014. [CrossRef]
10. Song, Y.; Xu, J.-L.; Liu, X.-X. Electrochemical anchoring of dual doping polypyrrole on graphene sheets partially exfoliated from graphite foil for high-performance supercapacitor electrode. *J. Power Sources* **2014**, *249*, 48–58. [CrossRef]
11. Tao, X.; Ye, S.; Zhu, K.; Dou, L.; Cui, P.; Ma, J.; Zhao, C.; Wei, X.; Guo, L.; Hojjati-Najafabadi, A.; et al. ATMP Doped Conductive PANI/CNTs Composite Hydrogel Electrodes toward High Energy Density Flexible Supercapacitors. *ACS Appl. Energy Mater.* **2023**, *6*, 8177–8188. [CrossRef]
12. Ma, M.; Du, X.; Chen, X.; Liang, S.; Liang, Z.; Li, Z.; Cao, X.; Huang, S.; Xie, Y.; Wang, S.; et al. Tubular Polypyrrole with Chloride Ion Dopants as an Ultrafast Organic Anode for High-Power Lithium-Ion Batteries. *ChemSusChem* **2023**, *16*, e202202174. [CrossRef]
13. Ullah, H.; Shah, A.-u.-H.A.; Bilal, S.; Ayub, K. Doping and Dedoping Processes of Polypyrrole: DFT Study with Hybrid Functionals. *J. Phys. Chem. C* **2014**, *118*, 17819–17830. [CrossRef]
14. Nguyen Ngoc, H.; Ngo Tuan, C.; Hoang Van, H.; Ha Manh, H.; Vu Quoc, T. Electronic properties of the polypyrrole-dopant anions ClO_4^- and MoO_4^{2-}: A density functional theory study. *J. Mol. Model.* **2017**, *23*, 336.
15. He, S.; Mukaida, M.; Kirihara, K.; Lyu, L.; Wei, Q. Reversible Protonic Doping in Poly(3,4-Ethylenedioxythiophene). *Polymers* **2018**, *10*, 1065. [CrossRef] [PubMed]
16. Xie, Y.; Xu, J.; Lu, L.; Xia, C. Electrochemical Investigation of Lithium Perchlorate-Doped Polypyrrole Growing on Titanium Substrate. *Inorganics* **2024**, *12*, 125. [CrossRef]
17. Alesary, H.F.; Ismail, H.K.; Khudhair, A.F.; Mohammed, M.Q. Effects of Dopant Ions on the Properties of Polyaniline Conducting Polymer. *Orient. J. Chem.* **2018**, *34*, 5. [CrossRef]
18. Alesary, H.F.; Ismail, H.K.; Mohammed, M.Q.; Mohammed, H.N.; Abbas, Z.K.; Barton, S. A comparative study of the effect of organic dopant ions on the electrochemical and chemical synthesis of the conducting polymers polyaniline, poly(o-toluidine) and poly(o-methoxyaniline). *Chem. Pap.* **2021**, *75*, 5087–5101. [CrossRef]
19. Motheo, A.J.; Santos, J.R.; Venancio, E.C.; Mattoso, L.H.C. Influence of different types of acidic dopant on the electrodeposition and properties of polyaniline films. *Polymer* **1998**, *39*, 6977–6982. [CrossRef]
20. Sayah, A.; Boumaza, N.; Habelhames, F.; Bahloul, A.; Tounsi, A.; Lamiri, L.; Nessark, B. Effect of dopant on electrochemical performance of polyaniline on FTO substrate. *Polym. Bull.* **2024**, *81*, 5179–5192. [CrossRef]
21. Ahamed, S.M.; Das, P.; Gupta, P.K.; Malik, S. Tetracarboxylic Acid-Doped Polyaniline Nanotubes: Effect of the Dopant Structure on the Morphology, Charge Storage Capacity, and Cycle Stability. *Energy Fuels* **2026**, *40*, 874–883. [CrossRef]
22. Jagtap, S.; Handore, K.; Adhav, P.; Deshpande, P.; Bhopale, A.; Khaladkar, M.; Khandagale, P.; Chabukswar, V.V. Room Temperature Operating, Fast and Reusable Polyaniline Sensor Synthesized Ultrasonically Using Organic and Inorganic Acid Dopants. *J. Macromol. Sci. Part B-Phys.* **2022**, *61*, 942–957. [CrossRef]
23. Xie, Y.; Yao, C. Interfacial effect investigation of lithium perchlorate-interacted oxygen-containing carbon paper. *Surf. Sci.* **2025**, *751*, 122615. [CrossRef]
24. Bao, W.; Yao, C.; Xie, Y. Electrochemical Measurement and Simulation of Sulfuric Acid-Doping Polyaniline on Graphite Carbon Paper. *Nano* **2024**, *19*, 2450099. [CrossRef]
25. Aykol, Ş.M.Ö.; Koçyiğit, N.; Davşan, L.T.; Yağci, Ö.; Arvas, M.B. Gold-nanoparticle/copolymer-modified screen printed carbon based electrode nonenzymatic electrochemical sensor for sensitive detection of pyocyanin as a Pseudomonas aeruginosa infections biomarker. *Microchem. J.* **2026**, *220*, 116393. [CrossRef]
26. Liu, Z.S.; Zhang, Z.Y.; Xie, W.Y.; Mao, Y.F.; Zhan, T. Fabrication of sisal fiber carbon paper-polyaniline composite as binder-free electrodes for supercapacitor. *Mater. Lett.* **2024**, *357*, 4. [CrossRef]
27. Choi, D.J.; Boscá, A.; Pedrós, J.; Martínez, J.; Barranco, V.; Rojo, J.M.; Yoo, J.J.; Kim, Y.H.; Calle, F. Improvement of the adhesion between polyaniline and commercial carbon paper by acid treatment and its application in supercapacitor electrodes. *Compos. Interfaces* **2016**, *23*, 133–143. [CrossRef]
28. Zhao, Z.; Xie, Y.; Lu, L. Electrochemical performance of polyaniline-derivated nitrogen-doped carbon nanowires. *Electrochim. Acta* **2018**, *283*, 1618–1631. [CrossRef]
29. Chen, Y.; Xie, Y. Electrochemical Performance of Manganese Coordinated Polyaniline. *Adv. Electron. Mater.* **2019**, *5*, 1900816. [CrossRef]

30. Rohom, A.B.; Londhe, P.U.; Mahapatra, S.K.; Kulkarni, S.K.; Chaure, N.B. Electropolymerization of polyaniline thin films. *High Perform. Polym.* **2014**, *26*, 641–646. [CrossRef]
31. Rahman, S.U.; Röse, P.; Surati, M.; Shah, A.U.A.; Krewer, U.; Bilal, S. 3D Polyaniline Nanofibers Anchored on Carbon Paper for High-Performance and Light-Weight Supercapacitors. *Polymers* **2020**, *12*, 2705. [CrossRef] [PubMed]

Disclaimer/Publisher's Note: The statements, opinions and data contained in all publications are solely those of the individual author(s) and contributor(s) and not of MDPI and/or the editor(s). MDPI and/or the editor(s) disclaim responsibility for any injury to people or property resulting from any ideas, methods, instructions or products referred to in the content.